Alternating-domain supersolids in binary dipolar condensates

T. Bland,[1,2] E. Poli,[2] L. A. Peña Ardila,[3] L. Santos,[3] F. Ferlaino,[1,2] and R. N. Bisset[2]

[1]*Institut für Quantenoptik und Quanteninformation,*
Österreichische Akademie der Wissenschaften, Innsbruck, Austria
[2]*Institut für Experimentalphysik, Universität Innsbruck, Austria*
[3]*Institut für Theoretische Physik, Leibniz Universität Hannover, Germany*
(Dated: December 1, 2022)

Two-component dipolar condensates are now experimentally producible, and we theoretically investigate the nature of supersolidity in this system. We predict the existence of a binary supersolid state in which the two components form a series of alternating domains, producing an immiscible double supersolid. Remarkably, we find that a dipolar component can even induce supersolidity in a nondipolar component. In stark contrast to single-component dipolar supersolids, alternating-domain supersolids do not require quantum stabilization, and the number of crystal sites is not strictly limited by the condensate populations, with the density hence being substantially lower. Our results are applicable to a wide range of dipole moment combinations, marking an important step towards long-lived bulk-supersolidity.

I. INTRODUCTION

The once elusive supersolid state of matter simultaneously exhibits superfluidity and crystalline order [1]. While early proposals sought superfluid properties of defects in a solid [2, 3], focusing on helium experiments [4], supersolidity has yet to be demonstrated in those systems [5]. It is instead the high-degree of flexibility and control offered by ultracold gases that led to the first observations of supersolidity, but of a different kind, with solid properties arising in superfluids. Supersolid features were observed in systems with cavity-mediated interactions [6], while supersolid stripes were realized with spin-orbit coupled Bose-Einstein condensates (BECs) [7, 8]. Supersolids have now been observed in experiments with dipolar BECs [9–11], and their superfluid character has been supported by the analysis of their excitations [12–14]. Note that supersolid proposals have also been made for gases with soft-core, finite range interactions [15–19].

The first dipolar supersolids were realized in single-component BECs in cigar-shaped traps, exhibiting a periodic density modulation along one direction [9–11], whereas experiments have now also created 2D supersolids with density modulations along two directions [20, 21]. From a theoretical perspective, there have been intriguing predictions for other exotic 2D supersolid states [22–27], as well as alluring manifestations of quantum vortices [28–30]. Dipolar supersolids may be created from unmodulated BECs by inducing a roton instability [9–11]. Dipolar rotons—constituting a local minimum of the energy dispersion at finite momenta due to the anisotropic and long-ranged dipole-dipole interactions [31, 32]—were first observed in cigar-shaped [33, 34] and then in pancake-shaped BECs [35]. An unstable roton mode seeds a periodic density modulation that can subsequently be stabilized by quantum fluctuations as the density grows, resulting in a supersolid [36, 37]. Recently, these same concepts were extended to the case of dipolar mixtures, i.e., systems composed of two dipolar components, which are now available in experiments [38–
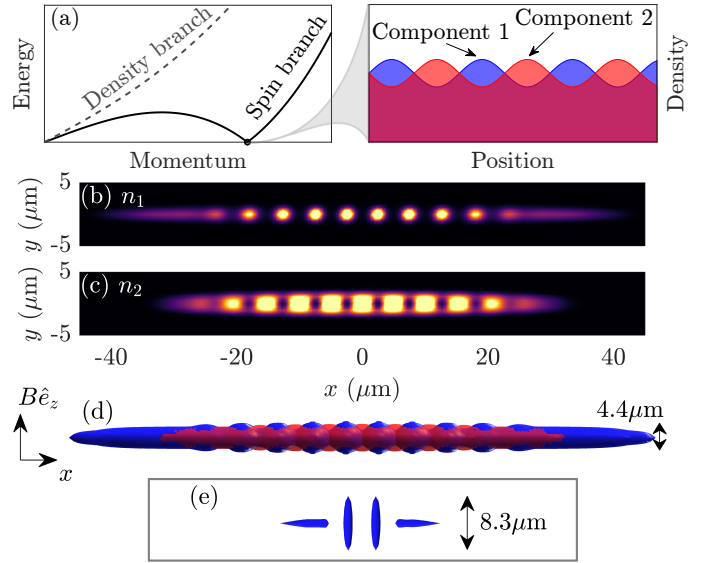

FIG. 1. (a) Dispersion relation schematic showing a roton instability in the spin branch with corresponding density modulations on the right for a dipolar mixture. (b-d) Alternating-domain supersolid for a dysprosium dipolar-nondipolar mixture. Column densities for (b) dipolar and (c) nondipolar components, with (d) double-isosurface plot at 2% of the peak density for each component. Interaction scattering lengths $(a_{11}, a_{12}, a_{22}) = (100, 98, 100)a_0$, trapping frequencies $\vec{f} = (5, 110, 150)$Hz, and populations $N_1 = N_2 = 1.5 \times 10^4$. (e) Corresponding single-component modulated state for the same trapping potential, $N = 3 \times 10^4$ and $a = 78a_0$. Subplots (b-e) are drawn to the same length scale.

40]. In particular, it was predicted that exotic supersolid states can be seeded by the addition of a second dipolar component [40, 41].

Dipolar mixtures, with their richness stemming from multiple sources of interactions, offer new phases with spontaneous modulation that go beyond quantum-fluctuation-stabilized supersolids. An early example pro-

posed that two immiscible BECs—displaced relative to one another by non-concentric confinement—might be used to realize a kind of binary supersolid formed by the instability of interface bending modes [42]. Binary dipolar BECs could also open another intriguing possibility. It was already predicted that unmodulated binary BECs may be destabilized by a spin roton mode [43, 44], for which a periodic density modulation develops in both components, but with the density maxima of one component occurring at the minima of the other [see Fig. 1(a)]. The key question is then, in analogy to the dipolar roton producing a single-component supersolid, could the unstable spin rotons point to a novel kind of supersolid?

In this article, we predict the existence of a phase, which we call an alternating-domain supersolid, that exists even at the mean-field level and does not require the regulatory action of quantum fluctuations. The two components form alternating domains, with a continuous superfluid connection within each component that periodically weaves through the other [see Fig. 1 (b-d)]. We uncover rich phase diagrams with broad regions in which both components are supersolid, as well as regions where a supersolid component is periodically punctuated by the isolated domains of the second component. We predict that the alternating-domain supersolid intrinsically relies on a dipolar imbalance between the two components, and can exist for far lower atom numbers and peak densities than quantum-stabilized supersolids, which has important implications for the potential size and longevity of supersolid crystals in realistic settings.

II. FORMALISM

We consider a three-dimensional system at zero temperature made of two bosonic components, $\sigma = \{1, 2\}$, consisting of atoms with permanent magnetic moments, although our work is also applicable to electric dipoles. Following Refs. [45, 46], we compute the Lee-Huang-Yang (LHY) energy density correction due to quantum fluctuations for a homogeneous binary mixture with densities $\mathbf{n} = (n_1, n_2)$:

$$\epsilon_{\text{LHY}}(\mathbf{n}) = \frac{16}{15\sqrt{2\pi}} \left(\frac{m}{4\pi\hbar^2} \right)^{3/2} \int_0^1 \mathrm{d}u \sum_{\lambda=\pm} V_\lambda(u, \mathbf{n})^{5/2} ,$$
(1)

where we assume equal masses $m = m_1 = m_2$, and

$$V_\pm(u, \mathbf{n}) = \sum_{\sigma=1,2} \alpha_{\sigma\sigma} n_\sigma \pm \sqrt{(\alpha_{11} n_1 - \alpha_{22} n_2)^2 + 4\alpha_{12}^2 n_1 n_2} .$$
(2)

Here, $\alpha_{\sigma\sigma'}(u) = g_{\sigma\sigma'} + g_{\sigma\sigma'}^d (3u^2 - 1)$, where the short-ranged and dipolar interaction parameters are, respectively, $g_{\sigma\sigma'} = 4\pi\hbar^2 a_{\sigma\sigma'}/m$ and $g_{\sigma\sigma'}^d = \mu_0\mu_\sigma\mu_{\sigma'}/3 = 4\pi\hbar^2 a_{\sigma\sigma'}^d/m$, with s-wave scattering lengths, $a_{\sigma\sigma'}$ and dipole moments μ_σ, where μ_0 is the vacuum permeability.

The wave function for each component Ψ_σ is obtained by solving the coupled extended Gross-Pitaevskii equations:

$$i\hbar \frac{\partial}{\partial t} \Psi_\sigma(\mathbf{x}) = \Bigg[-\frac{\hbar^2\nabla^2}{2m} + \frac{1}{2}m \left(\omega_x^2 x^2 + \omega_y^2 y^2 + \omega_z^2 z^2 \right)$$
$$+ \sum_{\sigma'} \int \mathrm{d}^3\mathbf{x}'\, U_{\sigma\sigma'}(\mathbf{x}' - \mathbf{x}) n_{\sigma'}(\mathbf{x}') + \sum_{\sigma'} g_{\sigma\sigma'} n_{\sigma'}(\mathbf{x})$$
$$+ \mu_{\text{LHY}}^{(\sigma)}[\mathbf{n}(\mathbf{x})] \Bigg] \Psi_\sigma(\mathbf{x}) ,$$
(3)

where $\omega_{x,y,z} = 2\pi f_{x,y,z}$ are the harmonic trapping frequencies, $U_{\sigma\sigma'}(\mathbf{r}) = \left[\mu_0\mu_\sigma\mu_{\sigma'}/4\pi r^3\right] \left(1 - 3\cos^2\theta\right)$ is the long-ranged anisotropic dipole-dipole interaction potential, with θ the angle between the polarization axis (always z) and the vector $\mathbf{r}$ that connects the two interacting particles, and $n_\sigma(\mathbf{x}) \equiv |\Psi_\sigma(\mathbf{x})|^2$ is the density of component σ, normalized to N_σ atoms. The last term in (3) is the quantum fluctuation correction to the chemical potential $\mu_{\text{LHY}}^{(\sigma)}[\mathbf{n}(\mathbf{x})] = \partial\epsilon_{\text{LHY}}(\mathbf{n}(\mathbf{x}))/\partial n_\sigma$, described within the local-density approximation framework.

III. ALTERNATING-DOMAIN SUPERSOLIDS

We demonstrate the unique features of alternating-domain supersolids by considering a dipolar-nondipolar mixture in Fig. 1, for which a combined total of 19 domains can be seen. While the dipolar component [Fig. 1(b)] can remain globally phase coherent through a continuous superfluid connection linking the domains—since we are close to the miscible-immiscible transition the separation is only partial—the nondipolar component [Fig. 1(c)] can also maintain a superfluid connection along high density rails encompassing the dipolar domains. The density isosurfaces in Fig. 1(d) highlight the shape of the dipolar domains, which are not as strongly elongated as the single-component case [cf. Fig. 1(e)]. While this concrete illustration considers two ^{164}Dy spin projections, with $(\mu_1, \mu_2) = (-10, 0)\mu_B$ for Bohr magneton μ_B, domain supersolids are not just a special feature of dipolar-nondipolar mixtures, but are rather general, as we discuss later.

These results must be contrasted to the single-component case. In Fig. 1(e) we show a modulated state for a single-component dipolar BEC for the same trap and total atom number as in Fig. 1(b-d), i.e., $N = 3\times10^4$. Note that we had to modify the scattering length, since $a = 100a_0$ corresponds to an unmodulated BEC. However, lowering to $a = 78a_0$ passes a transition to a modulated state that is not a supersolid, where the peak density $(4.0 \times 10^{21}\mathrm{m}^{-3})$ is immediately more than an order of magnitude larger than the domain supersolid case $(1.8 \times 10^{20}\mathrm{m}^{-3})$. Correspondingly, the number of atoms per lattice site is about an order of magnitude larger than for the domain supersolid. For this atom number and trap volume, the supersolid phase does not exist for the single-component case [27], which was also the situation for the regimes considered by Refs. [47–49].

To understand the physical mechanisms involved, it is instructive to consider the transition from unmodulated to modulated states. For the formation of a domain supersolid, the density modulation is triggered by unstable spin roton excitations [shown schematically in Fig. 1(a)], with wavelengths governed by the BEC's width along the direction of dipole polarization [43]. Spin modes act to increase the density difference, $|n_1 - n_2|$, and the instability is hence resolved once the components become spatially separated as alternating immiscible domains [[Figs. 1(b-d)]. Crucially, there is no significant increase of the total density $n_1 + n_2$, and the peak density can remain low. This situation should be contrasted to that of single component supersolids, and the two-component supersolids of Refs. [40, 41], for which a density roton instability would cause a divergence of the peak density if it were not counterbalanced by the appropriate LHY term [50], and this necessitates significantly higher densities [9–11]. Note that while single component supersolids require $a < a^d$, and thus are only stable due to quantum fluctuations [36, 37], domain supersolids can exist for either $a_{\sigma\sigma} > a^d_{\sigma\sigma}$ or $a_{\sigma\sigma} < a^d_{\sigma\sigma}$, but quantum fluctuations remain qualitatively important since, for example, if they were neglected the latter situation could only be at best metastable [51].

We focus on regimes where one component without the presence of the other will always be unmodulated, but each component within the binary system can exist in one of three phases: an unmodulated BEC, a supersolid state with a linear chain of domains (SS), or an array of isolated domains (ID). The distinction between these is set by upper-bound estimates for the superfluid fractions [52], which in our binary system are given by

$$f_{s,\sigma} = \frac{(2L)^2}{\int_{-L}^{L} dx\, \bar{n}_\sigma} \left[\int_{-L}^{L} \frac{dx}{\bar{n}_\sigma} \right]^{-1}, \quad \bar{n}_\sigma = \int_{-\infty}^{\infty} \int_{-\infty}^{\infty} dy dz\, n_\sigma,$$

for length L defined over the central region that encompasses the central 3 (4) domains if the number of domains is odd (even). We take the supersolid region to be when $f_{s,\sigma} > 0.1$ occurs concurrently with a periodic density modulation, following Ref. [53] for the arbitrary choice of $f_{s,\sigma} \leq 0.1$ defining the crossover to the regime of isolated domains. For reference, the superfluid fractions in Fig. 1 are (b) $f_{s,1} = 0.3032$, (c) $f_{s,2} = 0.7940$ and (e) $f_{s,1} = 0.0001$. Note, the total superfluid fraction $f_s = (N_1 f_{s,1} + N_2 f_{s,2})/N$ is associated with a reduction in the moment of inertia of the overall mixture. The periodic spatial ordering can be characterized by the density contrast $C_\sigma = (n_\sigma^{max} - n_\sigma^{min})/(n_\sigma^{max} + n_\sigma^{min})$, where n_σ^{max} (n_σ^{min}) are neighboring maxima (minima) as one moves along the trap's long direction. See Appendix A for more discussion on the calculation of the contrast. The boundary between unmodulated and modulated states is defined by C_σ changing from zero to a nonzero value.
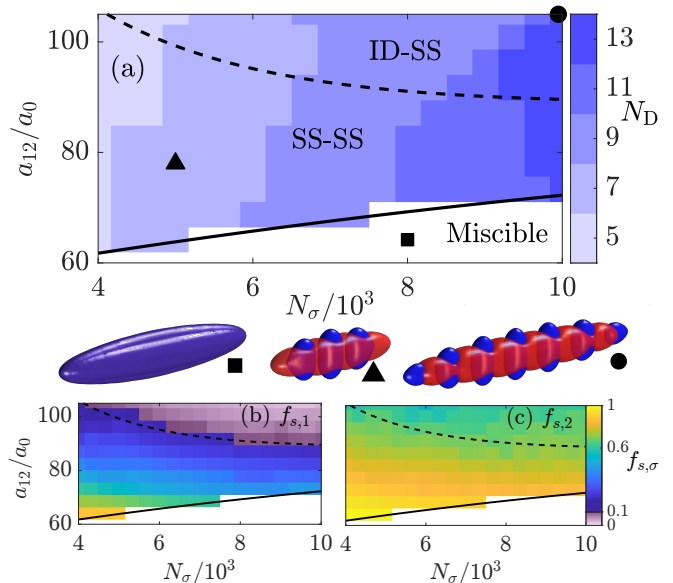

FIG. 2. Phase diagram for a dipolar-nondipolar mixture of ^{164}Dy atoms, varying intercomponent scattering length a_{12} and $N_1 = N_2 = N/2$ with fixed $N f_x$, from $f_x = 37.5$Hz on the left to $f_x = 15$Hz on the right. (a) Total number of domains in the stationary state solution. Solid lines separate unmodulated miscible to domain supersolid (SS-SS) state when $C_\sigma > 0$, and dashed line to isolated domains-supersolid (ID-SS) state. Example isosurfaces below are highlighted by the symbols in (a). (b,c) Superfluid fraction $f_{s,\sigma}$ of components 1 and 2. Threshold between SS and ID regime is indicated by a change of color scale. Other parameters: $a_{11} = a_{22} = 100 a_0$, $(\mu_1, \mu_2) = (-10, 0)\mu_B$, $f_y = f_z = 150$Hz.

IV. PHASE DIAGRAM FOR DIPOLAR-NONDIPOLAR MIXTURE

In Fig. 2 we explore the stationary state phase diagram of a dipolar-nondipolar mixture in a cigar-shaped trap with $(f_x, 150, 150)$Hz, $N_1 = N_2 = N/2$ and fixed $N f_x = 3 \times 10^5$Hz to maintain an approximately constant average density [27]. At low $a_{12} \lesssim 60 a_0$ the stationary state solution is a miscible unmodulated BEC, with only small deviation from perfect density overlap between components due to magnetostriction in the dipolar component [Fig. 2 ■]. Increasing a_{12} induces a transition to a domain supersolid state (SS-SS) [Fig. 2 ▲], where the domains of a given component exhibit a continuous superfluid connection [$f_{s,\sigma} > 0.1$ in Figs. 2(b)(c)]. We find that a quench of the intercomponent scattering length from the unmodulated miscible state to the domain supersolid regime generates a globally phase-coherent state—within each component—that is robust against the excitations induced by the quench, in-keeping with single-component studies of supersolids in a cigar-shaped geometry [9–11], which we detail in Appendix B [54]. Note how broad the SS-SS regime is, at least $20 a_0$ wide, compared to single-component supersolids where it is typically only a few a_0 wide [53]. Further increasing
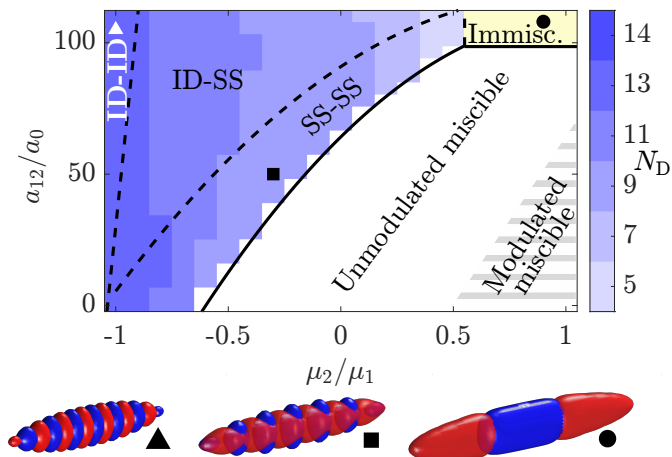
FIG. 3. Phase diagram for dipolar mixtures with varying inter-component scattering length and relative magnetic moment (note that $\mu_2/\mu_1 < 0$ implies antiparallel dipoles). Compared to Fig. 2, note the new phases: binary isolated domains (ID-ID), macroscopic-domain immiscibility (beige region), and the modulated miscible regime. Parameters: $N_1 = N_2 = 5 \times 10^3$, $a_{11} = a_{22} = 100a_0$, and $(f_x, f_y, f_z) = (15, 150, 150)$Hz.

a_{12} causes the overlap between components to reduce, expanding the distance between domains whilst decreasing superfluidity [Fig. 2(b)], crossing into the isolated domain-supersolid (ID-SS) regime [Fig. 2 ●]. However, the nondipolar component maintains a strong superfluid connection [Fig. 2(c)]. Note that the superfluid connection of component 2 can be controlled by adjusting f_y, with even a small reduction in f_y significantly reinforcing the nondipolar rails around the dipolar domains.

Figure 2(a) also shows how the total number of domains N_D changes in this phase diagram. Throughout, the average atom number per domain is $\sim 10^3$. Hence, as the atom number increases the number of domains climbs steadily, reaching a total of 13 once the system has 2×10^4 atoms (10^4 per component) on the far right-hand side. In contrast, single-component dipolar supersolids typically require $\sim 10^4$ atoms per lattice site [9–11].

V. GENERALIZATION TO VARIOUS DIPOLE COMBINATIONS

Here, we generalize our findings to mixtures in which both components can be dipolar, applicable to a wide range of experiments, e.g., erbium-dysprosium mixtures or spin mixtures of the same species. In Fig. 3, we construct a phase diagram by fixing μ_1 and exploring the effect of varying μ_2 and a_{12}. A solid line indicates a transition from a miscible to immiscible state, consistent with Fig. 2. For $\mu_2/\mu_1 < 0$ the dipoles are anti-aligned, decreasing the energy for dipoles of separate components to orient in the side-by-side configuration, thus causing both immiscibility and domain supersolidity to occur at
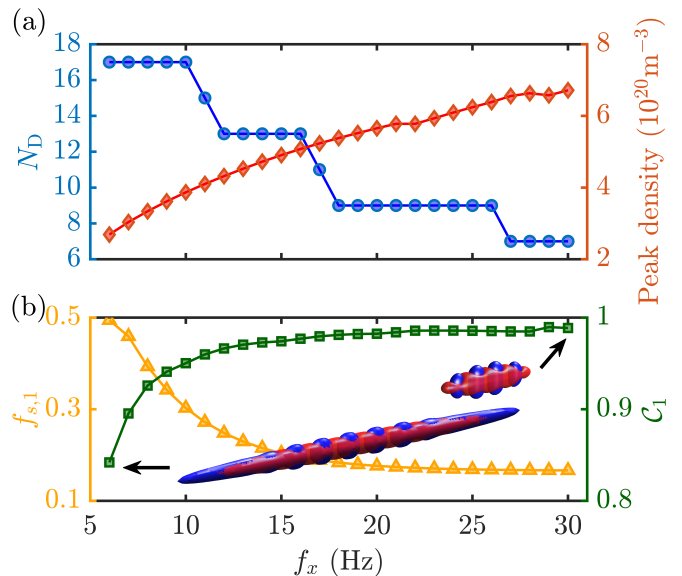

FIG. 4. Opening the trap for an erbium dipolar-nondipolar supersolid. (a) Reducing the long axis trap frequency, f_x, of a cigar-shaped trap increases the number of domains N_D whilst simultaneously reducing the peak density. (b) Superfluid fraction (density contrast, $\mathcal{C}_1$) of the dipolar component also increases (decreases), indicating an improving superfluid connection, whilst the second component is always a robust supersolid with the superfluid fraction never dropping below 0.7 (not shown). Parameters: $\mu_1 = -7\mu_B$ and $\mu_2 = 0$, $(a_{11}, a_{12}, a_{22}) = (65, 60, 65)a_0$, $N_1 = N_2 = 20000$ atoms, $f_y = f_z = 150$ Hz.

low a_{12} [Fig. 3 ■]. At $\mu_2/\mu_1 = -1$ the modulation is a perfect reflection about the $x = 0$ plane between the components, and for the range of a_{12} considered the system forms a binary isolated domain (ID-ID) state with 14 domains for only 10^4 atoms in total [Fig. 3 ▲].

For similar dipoles $\mu_2 \sim \mu_1$ there is little energy incentive from the dipolar interactions for the components to phase separate [44], hence the immiscibility boundary in Fig. 3 is close to the nondipolar result $a_{12} = \sqrt{a_{11}a_{22}} = 100a_0$, and the components separate to a macroscopic-domain immiscible state [43] [Fig. 3 ●]. While we focus on the immiscible domain regime, smaller $a_{\sigma\sigma}$ can trigger the formation of immiscible quantum-stabilized supersolids [40]. Miscible quantum-stabilized supersolids are also possible for smaller a_{12} following a density branch roton instability, indicated in the lower right corner of Fig. 3, which is explored further in Ref. [41]. If we instead considered $a_{\sigma\sigma} \geq a_{\sigma\sigma}^d$ we would expect qualitatively the same phases as in Fig. 3 apart for the modulated miscible phase.

VI. ULTRA-LOW DENSITY SUPERSOLIDS

We investigate weakening the axial confinement of a dipolar-nondipolar spin mixture of erbium, further

demonstrating the generality of our results to a broad range of dipole combinations. On the far right of Fig. 4 is a state in the SS-SS regime for $f_x = 30$Hz. Decreasing f_x to 6Hz increases the total number of domains from 7 to 17, whilst simultaneously reducing the peak density by a factor of ≈ 2.5. The increasing number of domains can be explained by the BEC becoming longer, while the spin roton wavelength is roughly fixed by the confinement length in the direction of dipole polarization. This behavior starkly contrasts with that for quantum-stabilized supersolids, which instead require a certain atom number for a given trap volume [27], and the supersolid regime is not possible if this criterion is not met [47–49]. For example, recall the modulated state in Fig. 1(e), for which the atom number is insufficient for this trap to attain supersolidity. Whilst decreasing f_x the superfluid fraction is monotonically increased from close to the ID-SS to deep in the SS-SS regime. These results are compared to the density contrast, which shows an improved density linking between domains (smaller $\mathcal{C}_\sigma$) for looser confinement.

VII.   CONCLUSIONS

We predict an alternating-domain supersolid state in two-component dipolar condensates. This binary supersolid exists over a broad region of parameter space and, importantly, it is robust against the excitations caused by crossing the unmodulated BEC–to–domain supersolid transition. There is also a crossover to an adjacent region where one of the components is supersolid, but the other forms isolated domains. In contrast to single-component supersolids–which must be stabilized by quantum fluctuations–alternating-domain supersolids

can produce numerous lattice sites with relatively small atom numbers, and have similar peak densities to unmodulated BECs, important for their longevity, which is largely determined by the inelastic three-body collisions that depend strongly on the density [37].

Our results are applicable to various dipole moment combinations, such as spin mixtures or binary gases comprised of two atomic species. Interestingly, we even find that a dipolar component can induce supersolidity within a non-dipolar component via their mutual interactions. Our work opens the door for future investigations into binary supersolid states and their excitations, as well as the exploration of novel 2D domain supersolids with exotic structures and vortex states. Our results reveal a rich system, within current experimental reach, and mark an important step towards long-lived bulk-supersolidity.

Note added.—Very recently, we became aware of a simultaneously submitted work addressing supersolidity in an immiscible dipolar-nondipolar mixture [55].

[1] M. Boninsegni and N. V. Prokof'ev, Colloquium: Supersolids: What and where are they?, Reviews of Modern Physics **84**, 759 (2012).

[2] E. P. Gross, Unified theory of interacting bosons, Physical Review **106**, 161 (1957).

[3] A. Andreev and I. Lifshitz, Quantum theory of defects in crystals, Zh. Eksp. Teor. Fiz. **56**, 2057 (1969).

[4] E. Kim and M. Chan, Probable observation of a supersolid helium phase, Nature **427**, 225 (2004).

[5] D. Y. Kim and M. H. W. Chan, Absence of supersolidity in solid helium in porous vycor glass, Phys. Rev. Lett. **109**, 155301 (2012).

[6] J. Léonard, A. Morales, P. Zupancic, T. Esslinger, and T. Donner, Supersolid formation in a quantum gas breaking a continuous translational symmetry, Nature **543**, 87 (2017).

[7] J.-R. Li, J. Lee, W. Huang, S. Burchesky, B. Shteynas, F. Ç. Top, A. O. Jamison, and W. Ketterle, A stripe phase with supersolid properties in spin–orbit-coupled bose–einstein condensates, Nature **543**, 91 (2017).

[8] T. M. Bersano, J. Hou, S. Mossman, V. Gokhroo, X.-W. Luo, K. Sun, C. Zhang, and P. Engels, Experimental realization of a long-lived striped bose-einstein condensate induced by momentum-space hopping, Phys. Rev. A **99**, 051602 (2019).

[9] L. Tanzi, E. Lucioni, F. Famà, J. Catani, A. Fioretti, C. Gabbanini, R. N. Bisset, L. Santos, and G. Modugno, Observation of a dipolar quantum gas with metastable supersolid properties, Phys. Rev. Lett. **122**, 130405 (2019).

[10] F. Böttcher, J.-N. Schmidt, M. Wenzel, J. Hertkorn, M. Guo, T. Langen, and T. Pfau, Transient supersolid properties in an array of dipolar quantum droplets, Phys. Rev. X **9**, 011051 (2019).

[11] L. Chomaz, D. Petter, P. Ilzhöfer, G. Natale, A. Trautmann, C. Politi, G. Durastante, R. M. W. van Bijnen, A. Patscheider, M. Sohmen, M. J. Mark, and F. Ferlaino, Long-lived and transient supersolid behaviors in dipolar quantum gases, Phys. Rev. X **9**, 021012 (2019).

[12] G. Natale, R. van Bijnen, A. Patscheider, D. Petter, M. Mark, L. Chomaz, and F. Ferlaino, Excitation spec-

trum of a trapped dipolar supersolid and its experimental evidence, Phys. Rev. Lett. **123**, 050402 (2019).

[13] L. Tanzi, S. Roccuzzo, E. Lucioni, F. Famà, A. Fioretti, C. Gabbanini, G. Modugno, A. Recati, and S. Stringari, Supersolid symmetry breaking from compressional oscillations in a dipolar quantum gas, Nature **574**, 382 (2019).

[14] M. Guo, F. Böttcher, J. Hertkorn, J.-N. Schmidt, M. Wenzel, H. P. Büchler, T. Langen, and T. Pfau, The low-energy goldstone mode in a trapped dipolar supersolid, Nature **574**, 386 (2019).

[15] F. Cinti, P. Jain, M. Boninsegni, A. Micheli, P. Zoller, and G. Pupillo, Supersolid droplet crystal in a dipole-blockaded gas, Phys. Rev. Lett. **105**, 135301 (2010).

[16] S. Saccani, S. Moroni, and M. Boninsegni, Phase diagram of soft-core bosons in two dimensions, Phys. Rev. B **83**, 092506 (2011).

[17] S. Saccani, S. Moroni, and M. Boninsegni, Excitation spectrum of a supersolid, Phys. Rev. Lett. **108**, 175301 (2012).

[18] M. Kunimi and Y. Kato, Mean-field and stability analyses of two-dimensional flowing soft-core bosons modeling a supersolid, Phys. Rev. B **86**, 060510 (2012).

[19] T. Macrì, F. Maucher, F. Cinti, and T. Pohl, Elementary excitations of ultracold soft-core bosons across the superfluid-supersolid phase transition, Phys. Rev. A **87**, 061602 (2013).

[20] M. A. Norcia, C. Politi, L. Klaus, E. Poli, M. Sohmen, M. J. Mark, R. N. Bisset, L. Santos, and F. Ferlaino, Two-dimensional supersolidity in a dipolar quantum gas, Nature **596**, 357–361 (2021).

[21] T. Bland, E. Poli, C. Politi, L. Klaus, M. Norcia, F. Ferlaino, L. Santos, and R. Bisset, Two-dimensional supersolid formation in dipolar condensates, Phys. Rev. Lett. **128**, 195302 (2022).

[22] R. Bombin, J. Boronat, and F. Mazzanti, Dipolar bose supersolid stripes, Phys. Rev. Lett. **119**, 250402 (2017).

[23] D. Baillie and P. B. Blakie, Droplet crystal ground states of a dipolar bose gas, Phys. Rev. Lett. **121**, 195301 (2018).

[24] Y.-C. Zhang, F. Maucher, and T. Pohl, Supersolidity around a critical point in dipolar bose-einstein condensates, Phys. Rev. Lett. **123**, 015301 (2019).

[25] Y.-C. Zhang, T. Pohl, and F. Maucher, Phases of supersolids in confined dipolar bose-einstein condensates, Phys. Rev. A **104**, 013310 (2021).

[26] J. Hertkorn, J.-N. Schmidt, M. Guo, F. Böttcher, K. S. H. Ng, S. D. Graham, P. Uerlings, T. Langen, M. Zwierlein, and T. Pfau, Pattern formation in quantum ferrofluids: From supersolids to superglasses, Phys. Rev. Research **3**, 033125 (2021).

[27] E. Poli, T. Bland, C. Politi, L. Klaus, M. A. Norcia, F. Ferlaino, R. N. Bisset, and L. Santos, Maintaining supersolidity in one and two dimensions, Phys. Rev. A **104**, 063307 (2021).

[28] A. Gallemí, S. Roccuzzo, S. Stringari, and A. Recati, Quantized vortices in dipolar supersolid bose-einstein-condensed gases, Phys. Rev. A **102**, 023322 (2020).

[29] S. Roccuzzo, A. Gallemí, A. Recati, and S. Stringari, Rotating a supersolid dipolar gas, Phys. Rev. Lett. **124**, 045702 (2020).

[30] F. Ancilotto, M. Barranco, M. Pi, and L. Reatto, Vortex properties in the extended supersolid phase of dipolar bose-einstein condensates, Phys. Rev. A **103**, 033314 (2021).

[31] D. H. J. O'Dell, S. Giovanazzi, and G. Kurizki, Rotons in gaseous bose-einstein condensates irradiated by a laser, Phys. Rev. Lett. **90**, 110402 (2003).

[32] L. Santos, G. Shlyapnikov, and M. Lewenstein, Roton-maxon spectrum and stability of trapped dipolar bose-einstein condensates, Phys. Rev. Lett. **90**, 250403 (2003).

[33] L. Chomaz, R. M. W. van Bijnen, D. Petter, G. Faraoni, S. Baier, J. H. Becher, M. J. Mark, F. Wächtler, L. Santos, and F. Ferlaino, Observation of roton mode population in a dipolar quantum gas, Nature Physics **14**, 442 (2018).

[34] D. Petter, G. Natale, R. M. W. van Bijnen, A. Patscheider, M. J. Mark, L. Chomaz, and F. Ferlaino, Probing the roton excitation spectrum of a stable dipolar bose gas, Phys. Rev. Lett. **122**, 183401 (2019).

[35] J.-N. Schmidt, J. Hertkorn, M. Guo, F. Böttcher, M. Schmidt, K. S. Ng, S. D. Graham, T. Langen, M. Zwierlein, and T. Pfau, Roton excitations in an oblate dipolar quantum gas, Phys. Rev. Lett. **126**, 193002 (2021).

[36] F. Böttcher, J.-N. Schmidt, J. Hertkorn, K. S. H. Ng, S. D. Graham, M. Guo, T. Langen, and T. Pfau, New states of matter with fine-tuned interactions: quantum droplets and dipolar supersolids, Reports on Progress in Physics **84**, 012403 (2020).

[37] L. Chomaz, I. Ferrier-Barbut, F. Ferlaino, B. Laburthe-Tolra, B. L. Lev, and T. Pfau, Dipolar physics: A review of experiments with magnetic quantum gases, arXiv preprint arXiv:2201.02672 (2022).

[38] A. Trautmann, P. Ilzhöfer, G. Durastante, C. Politi, M. Sohmen, M. J. Mark, and F. Ferlaino, Dipolar quantum mixtures of erbium and dysprosium atoms, Phys. Rev. Lett. **121**, 213601 (2018).

[39] G. Durastante, C. Politi, M. Sohmen, P. Ilzhöfer, M. J. Mark, M. A. Norcia, and F. Ferlaino, Feshbach resonances in an erbium-dysprosium dipolar mixture, Phys. Rev. A **102**, 033330 (2020).

[40] C. Politi, A. Trautmann, P. Ilzhöfer, G. Durastante, M. Mark, M. Modugno, and F. Ferlaino, Interspecies interactions in an ultracold dipolar mixture, Phys. Rev. A **105**, 023304 (2022).

[41] D. Scheiermann, L. A. Peña Ardila, T. Bland, R. N. Bisset, and L. Santos, Catalyzation of supersolidity in binary dipolar condensates, arXiv preprint arXiv:2202.08259 (2022).

[42] H. Saito, Y. Kawaguchi, and M. Ueda, Ferrofluidity in a two-component dipolar bose-einstein condensate, Phys. Rev. Lett. **102**, 230403 (2009).

[43] R. M. Wilson, C. Ticknor, J. L. Bohn, and E. Timmermans, Roton immiscibility in a two-component dipolar bose gas, Phys. Rev. A **86**, 033606 (2012).

[44] A.-C. Lee, D. Baillie, P. Blakie, and R. Bisset, Miscibility and stability of dipolar bosonic mixtures, Phys. Rev. A **103**, 063301 (2021).

[45] R. N. Bisset, L. A. P. Ardila, and L. Santos, Quantum droplets of dipolar mixtures, Phys. Rev. Lett. **126**, 025301 (2021).

[46] J. C. Smith, D. Baillie, and P. B. Blakie, Quantum droplet states of a binary magnetic gas, Phys. Rev. Lett. **126**, 025302 (2021).

[47] H. Kadau, M. Schmitt, M. Wenzel, C. Wink, T. Maier, I. Ferrier-Barbut, and T. Pfau, Observing the rosensweig instability of a quantum ferrofluid, Nature **530**, 194 (2016).

[48] F. Wächtler and L. Santos, Quantum filaments in dipolar bose-einstein condensates, Phys. Rev. A **93**, 061603 (2016).

[49] R. N. Bisset, R. M. Wilson, D. Baillie, and P. B. Blakie, Ground-state phase diagram of a dipolar condensate with quantum fluctuations, Phys. Rev. A **94**, 033619 (2016).

[50] A. R. P. Lima and A. Pelster, Quantum fluctuations in dipolar bose gases, Phys. Rev. A **84**, 041604 (2011).

[51] If quantum fluctuations are neglected, $a < a^d$ generally means that dipolar condensates can only be metastable [56].

[52] A. J. Leggett, Can a solid be "superfluid"?, Phys. Rev. Lett. **25**, 1543 (1970).

[53] P. Blakie, D. Baillie, L. Chomaz, and F. Ferlaino, Supersolidity in an elongated dipolar condensate, Physical Review Research **2**, 043318 (2020).

[54] https://youtu.be/jUxQCbEZiZM.

[55] S. Li, U. N. Le, and H. Saito, Long-lifetime supersolid in a two-component dipolar bose-einstein condensate, Phys. Rev. A **105**, L061302 (2022).

[56] T. Lahaye, C. Menotti, L. Santos, M. Lewenstein, and T. Pfau, The physics of dipolar bosonic quantum gases, Rep. Prog. Phys. **72**, 126401 (2009).

[57] P. Ilzhöfer, M. Sohmen, G. Durastante, C. Politi, A. Trautmann, G. Natale, G. Morpurgo, T. Giamarchi, L. Chomaz, M. Mark, *et al.*, Phase coherence in out-of-equilibrium supersolid states of ultracold dipolar atoms, Nature Physics **17**, 356 (2021).

Appendix A: Density contrast

The onset of periodic density modulation is characterized by the density contrast, akin to interferometric visibility, defined as

$$\mathcal{C}_\sigma = \frac{n_\sigma^{\max} - n_\sigma^{\min}}{n_\sigma^{\max} + n_\sigma^{\min}} \qquad (A1)$$

for each bosonic component $\sigma = \{1, 2\}$ and where $n_\sigma^{\max}$ and $n_\sigma^{\min}$ are neighboring maxima and minima in the 3D density as one moves along the long direction of the trap. In Fig. 5 we graphically depict the line of maximum 3D density in the $z = 0$ plane, showing the maxima (red circles) and minima (green crosses) in the density along this curve. Typically, for the component with a larger dipole moment this curve lies along $y = 0$, just as it does for single-component supersolids [9–11]. However, the nondipolar component has a greater superfluid connection along the rails, a feature which can be captured by our generalization of Eq. (A1). This connection can still be lost, however, through tightening f_y, for example.

Appendix B: Dynamic preparation

The preparation of a single-component supersolid has been achieved through either taking an unmodulated BEC and quenching the scattering length across the unmodulated BEC-to-supersolid transition [9–11], or by direct evaporative cooling into the supersolid state [11, 20,
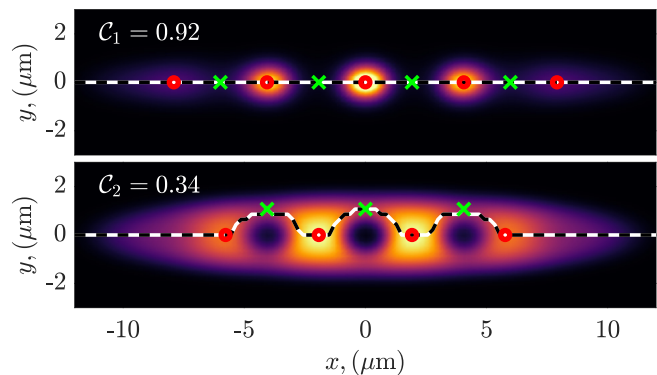

FIG. 5. Contrast $\mathcal{C}_\sigma$ of a dipolar-nondipolar mixture of ^{164}Dy atoms. Dashed line indicates the y position of the maximum density along x. Red circles are the peaks ($n_\sigma^{\max}$) and green crosses the troughs ($n_\sigma^{\min}$) of density along the dashed line. Other parameters: $(\mu_1, \mu_2) = (-10, 0)\mu_B$, $N_1 = N_2 = N/2 = 7000$, $a_{12} = 70a_0$, $a_{11} = a_{22} = 100a_0$, $(f_x, f_y, f_z) = (21, 150, 150)$Hz.

21]. The two-component case affords a wide range of possibilities for domain supersolid preparation, due to the large number of tunable interaction parameters in the system. Here, we investigate one possibility through tuning the intercomponent scattering length a_{12}. Taking an initially unmodulated miscible dipolar-nondipolar mixture with the parameters from Fig. 5 and $a_{12} = 65a_0$, we simulate an instantaneous quench to $a_{12} = 70a_0$. The consequent dynamics are shown in Fig. 6. Despite the violent nature of the instantaneous quench, the system maintains phase coherence throughout the lifetime of the simulation, as indicated by the blue (red) isosurface for component 1 (2), and the solution resembles the target stationary solution [Fig. 5]. We also include a Supplementary Video of the dynamics [54].
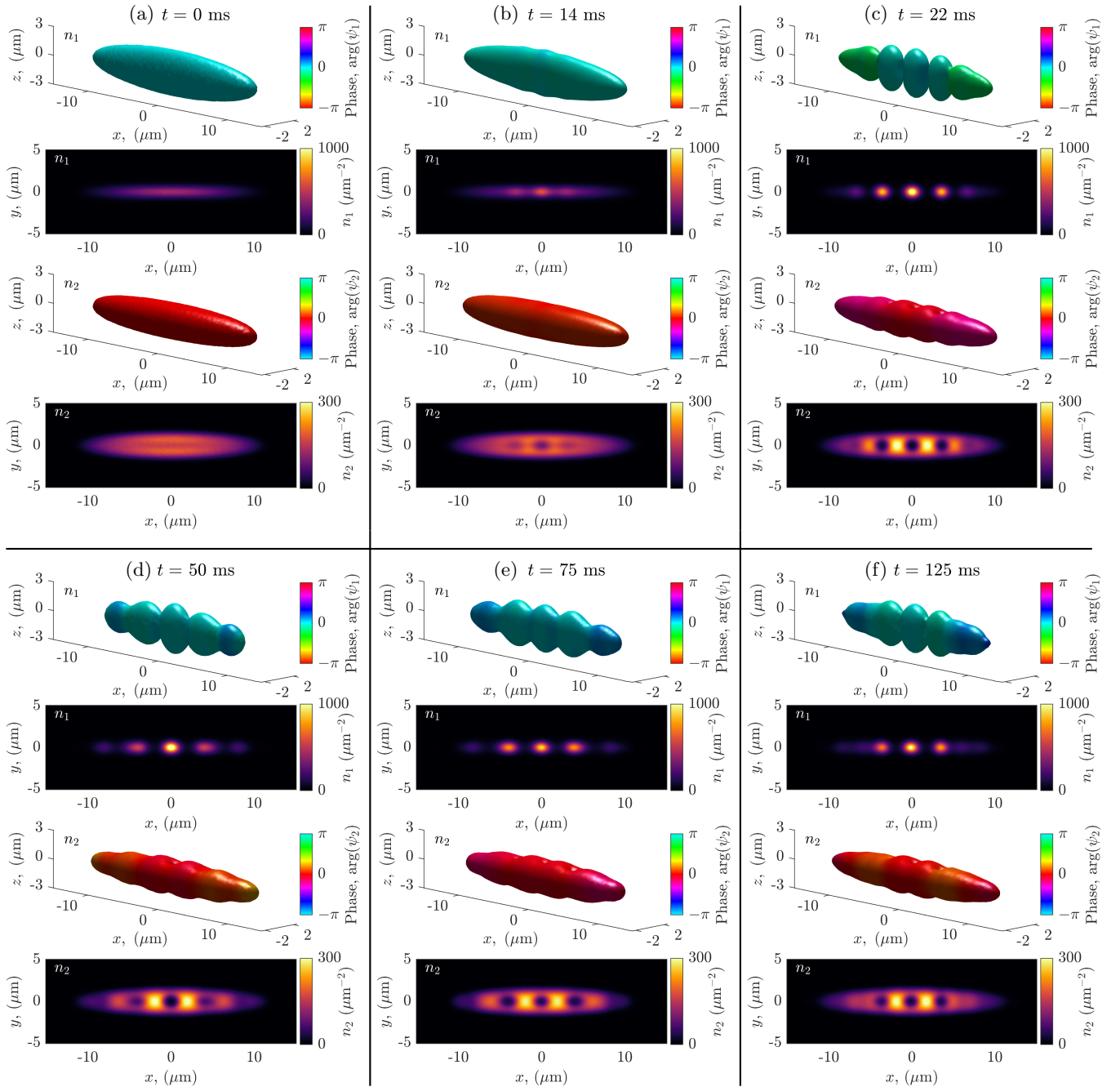
FIG. 6. Preparation of a domain supersolid through an interaction quench. Simulation of an instantaneous quench from $a_{12} = 65a_0$ to $a_{12} = 70a_0$ at $t = 0$, with other parameters from Fig. 5. Each labeled frame corresponds to a time during the consequent dynamics, and within each frame the data can be understood row-by-row. Row 1: 5% density isosurface for component 1 colored to the phase, and centered such that the phase at the origin is 0, perfect coherence for component 1 would be light blue. Row 2: Column density for component 1 normalized to peak value over the whole simulation. Row 3: same as Row 1 but for the second component, but perfect coherence in component 2 would be red. Row 4: same as Row 2 but for the second component, with a smaller peak density. Note that the stationary solution for the final parameters is the state presented in Fig. 5. A Supplementary Video of this simulation is also included [54].
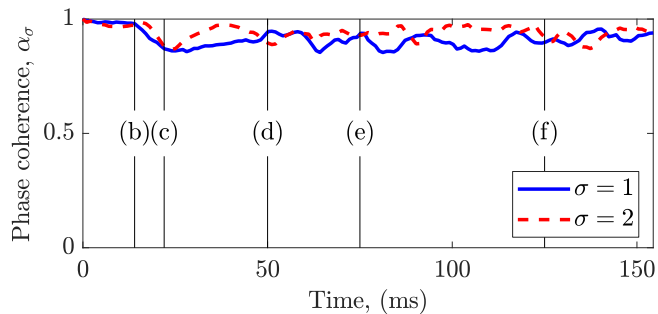
FIG. 7. Phase coherence α_σ for each component $\sigma = \{1, 2\}$ following an instantaneous quench from an unmodulated miscible BEC to a domain supersolid state. Labels in the plot coincide with the frames shown in Fig. 6.

We can dynamically characterize the supersolid quality by plotting the phase coherence over time. Following Ref. [9] (see also Refs. [21, 57]) we define the phase coherence as

$$\alpha_\sigma = 1 - \frac{2}{\pi} \frac{\int_{\mathcal{R}} \mathrm{d}x\mathrm{d}y\, |\psi_\sigma(x,y)|^2 |\theta_\sigma(x,y) - \beta|}{\int_{\mathcal{R}} \mathrm{d}x\mathrm{d}y\, |\psi_\sigma(x,y)|^2}, \quad \text{(B1)}$$

where $\theta_\sigma(x,y)$ is the phase of $\psi_\sigma(x,y)$ in the $z = 0$ plane, and β is a fitting parameter to maximize α_σ at each time. The integration region $\mathcal{R}$ encompasses the cloud. From this definition $\alpha_\sigma = 1$ corresponds to perfect phase coherence across the BEC. In Fig. 7 we present the dynamical evolution of the phase coherence after the instantaneous quench presented in Fig. 6. Throughout the total time evolution, α_σ does not go below 0.85 for either component, suggesting excellently maintained phase coherence.